aerospace

MDPI

Article

Contrast Icing Wind Tunnel Tests between Normal Droplets and Supercooled Large Droplets

Zhirong Han *, Jiangtao Si and Dawei Wu

Shanghai Aircraft Design and Research Institute, Shanghai 201210, China
* Correspondence: hanzhirong@comac.cc

Abstract: In order to compare and analyze the similarities and differences between normal droplet icing shapes and supercooled large droplet icing shapes, SADRI carried out normal droplet and supercooled large droplet icing wind tunnel tests in the NRC−AIWT icing wind tunnel. Taking the typical glaze ice in normal droplet icing conditions as the reference, the freezing drizzle and freezing rain icing tests under the supercooled large droplet conditions were carried out. The test results show that compared with normal droplets, the ice horn height of supercooled large droplets decreases with the increase in droplet particle size, and even the ice horn characteristics are not obvious when the icing condition is freezing rain. At the same time, the range and height of rough element ice shape after the main ice horn of supercooled large droplets are significantly larger and higher than those of the normal droplets, while the difference in the rough element in different supercooled large droplet icing conditions is small.

Keywords: supercooled large droplets; icing wind tunnel tests; glaze ice; freezing rain; rough element

Citation: Han, Z.; Si, J.; Wu, D. Contrast Icing Wind Tunnel Tests between Normal Droplets and Supercooled Large Droplets. *Aerospace* **2022**, *9*, 844. https://doi.org/10.3390/aerospace9120844

Academic Editors: Dan Zhao, Chenzhen Ji and Hexia Huang

Received: 25 November 2022
Accepted: 16 December 2022
Published: 18 December 2022

1. Introduction

When a plane crosses clouds containing supercooled droplets which hit the surface, the droplets will ice and accrete on the surface when the temperature is below freezing. Ice not only changes the aerodynamic configuration of the aircraft (especially on the wings), it has a bad impact on the handling and stability of the aircraft, but also may fall off into the engine or hit the body. So, aircraft icing is one of the main threats to flight safety [1]. Johnson stated [2], "The icing problem is one of the most important ones facing the aviation industry today". In 1938, Gulick [3] tested an aspect ratio 6 wing in the Langley Full-Scale Tunnel with roughness intended to simulate an ice accretion. He found a 25% reduction in maximum lift and a 90% increase in drag for the conditions tested. Therefore, icing seriously affects the flight safety of aircraft. As for supercooled large droplet (SLD) ice, Ashenden et al. [4] found a similar result in wind tunnel tests with simulated ice accretions. The results showed more severe aerodynamic penalties due to the freezing drizzle case when operation of the deicing boot was simulated. Lee and Bragg [5] found that when the simulated ice shape was located at critical chordwise locations, a long separation bubble formed downstream of the shape and effectively eliminated the formation of a large leading-edge suction peak that was observed on the clean NACA 23012 airfoil. This resulted in a significant reduction in the maximum lift coefficient. For more information on the impact of icing on aircraft aerodynamics, refer to Reference [6].

Currently, civil aviation bureaus attach great importance to the safety of aircraft icing. In the airworthiness regulations of transport aircraft, there are a large number of items concerning the flight safety under icing conditions [7,8].

On 31 October 1994, an ATR72 model transport aircraft was wrecked in icing weather conditions [9]. The NTSB investigated the accident and confirmed that the cause of the accident was local freezing rain weather conditions that exceeded the normal drop icing environment in the FAA airworthiness regulations (Appendix C icing environment). Later,

after 20 years of meteorological research, the FAA officially issued a new airworthiness icing requirement (the 140 amendment) in 2014, adding Appendix O SLD icing conditions.

With the release of new airworthiness regulations and the increasing importance of the icing status and anti/de-icing devices under SLD icing conditions, the analysis and test verification methods of icing conditions in SLD also face new challenges [10–16]. Numerical simulation and icing wind tunnel experiments are the common methods to verify the aerodynamic performance and the effect of anti/de-icing devices under icing conditions. When the aircraft manufacturer indicates the aircraft's compliance with airworthiness to a civil aviation bureau, it generally needs to use more than one method to verify safety. For flight safety under icing conditions, an icing wind tunnel test is one of the most important methods. When additional SLD icing conditions are added to the airworthiness regulations, the icing wind tunnel test becomes one of the most important and feasible means to understand the similarities and differences between the normal droplet ice shape and SLD ice shape. The icing wind tunnel can be used in any season with stable test conditions and good repeatability. Compared with the natural icing test and icing tank test, the cost is low and the test period is short, and is very safe. However, the test capability envelope is limited, subject to the capability of the test equipment. At present, the icing wind tunnel test plays an irreplaceable role in solving the three-dimensional icing ice type prediction, verifying the effect of the anti/de-icing device, and verifying the accuracy of the numerical simulation results [17–20].In order to obtain the similarities and differences between frozen ice shapes and SLD ice freezing conditions, the Shanghai Aircraft Design and Research Institute has carried out a phase of normal droplets and SLD at the high-Altitude Icy Wind Tunnel (AIWT) of the National Research Council of Canada (NRC) [21,22] to compare the icy air tunnel tests.

2. Icing Wind Tunnel

The AIWT belonging to the NRC is a refrigerated closed-loop low-speed wind tunnel oriented in a vertical plane as shown in Figure 1. The wind tunnel has two available test section sizes of 0.57 m × 0.57 m, with a demonstrated top simulated wind speed of over 100 m/s, and 0.52 m × 0.33 m, that increases the top wind speed to 180 m/s. The wind tunnel has a height simulation capacity of 0~9100 m [10]. The air temperature in the AIWT is controlled by varying the amount of refrigerant flowing through the heat exchanger in the channel loop to achieve a static air temperature at a Mach number of 0.3, ranging from −40 °C to + 30 °C or higher. The pressure in the wind tunnel can be controlled between about 101 and 30 kPa, which allows the simulation to rise from the ground to at least 40,000 ft. The wind tunnel uses 2 nozzle systems to simulate the icing conditions of SLD [23,24]. The small nozzle and large nozzle each have a set of independent water supply and gas supply systems. In the development of SLD icing condition simulation ability, the wind tunnel researchers first used computational methods to simulate the granularity distribution characteristics obtained by two nozzle joint injections with Langmuir-D distribution, and compared them with the curve of Appendix O to obtain the calculation results very close to the Appendix O curve in FAA Amendment 140. Based on the calculation results, the verification work of the combined jet in the wind tunnel was conducted. By continuously adjusting the water supply and gas supply pressure of the nozzle, the bimodal distribution characteristics consistent with the SLD conditions were well realized, as shown in Figure 2. The "App. O ZLE < 40" represents mean volume diameter (MVD) of freezing drizzle (FZDZ) less than 40 μm. The "App. O ZRE < 40" represents mean volume diameter (MVD) of freezing rain (FZRA) less than 40 μm.

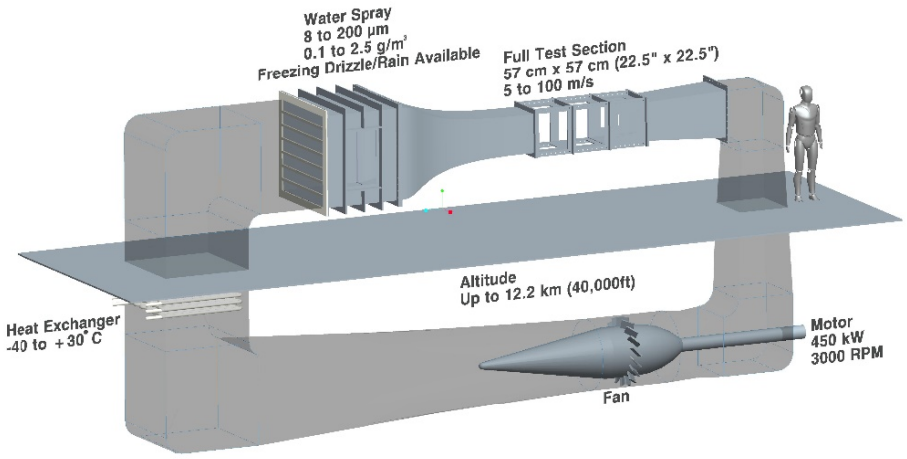

Figure 1. NRC−AIWT schematic diagram.

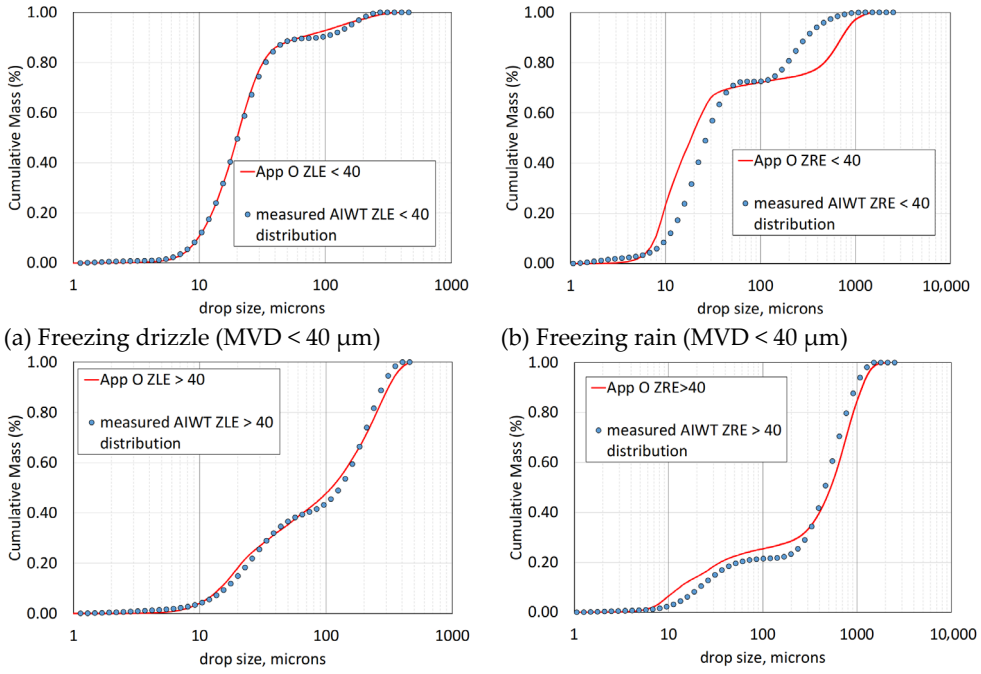

(a) Freezing drizzle (MVD < 40 μm)

(b) Freezing rain (MVD < 40 μm)

(c) Freezing drizzle (MVD ≥ 40 μm)

(d) Freezing rain (MVD ≥ 40 μm)

Figure 2. NRC−AIWT drop cumulative mass distribution for freezing drizzle and freezing rain.

3. Model

Considering the blockage in the icing wind tunnel in the 0.57 m × 0.57 m test section, a NACA0012 airfoil with 0.533 m chord length and 0.565 m span length was selected as the test model as shown in Figure 3 with details. The model was designed and manufactured by the NRC. The model has two leading edges, one is equipped with pressure taps as shown in Figure 4 to match the angle of attack by measuring the upper and lower surface pressure distribution. The other leading edge is for all icing tests. As shown in Figure 5, to reduce the weight, the first 1/4 of the airfoil is made of aluminum alloy (hollowed out), and the aft 3/4 of the airfoil is made of acrylic.

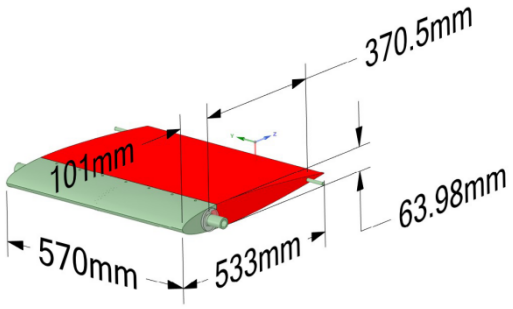

Figure 3. Test model and size.

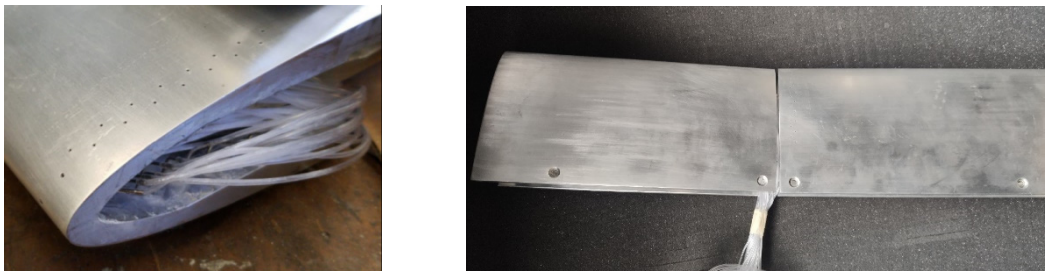

Figure 4. Pressure taps at one leading edge.

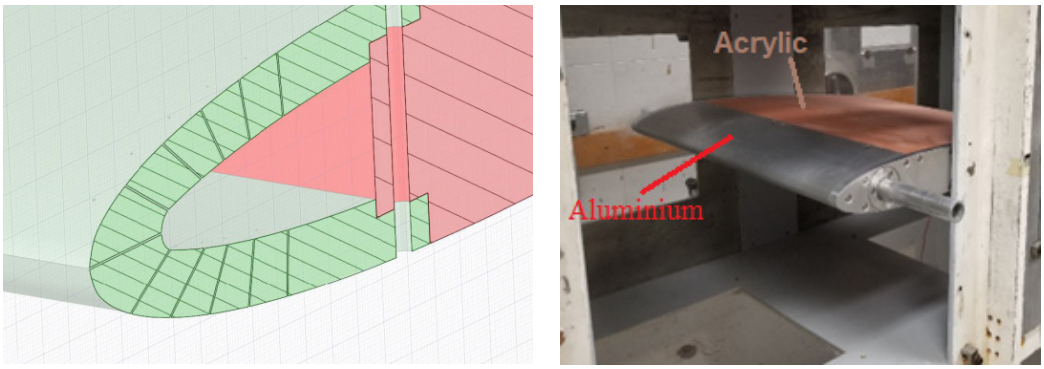

Figure 5. Two different materials of the model: aluminium alloy (hollowed out) and acrylic.

4. Test Conditions

The tests were performed in accordance with Appendixes C and O of CFR 14 Part 25. It should be noted that the AIWT does not fully guarantee that the in-flight icing simulation meets the Appendix O conditions due to the difficult decreasing temperature and velocity balance with the surrounding airflow.

As shown in Table 1, the test conditions include 10 test points (excluding repetitive runs). Target test points include the following conditions: (1) Appendix C [25,26] (double ice horns and single ice horn); (2) Appendix O glaze ice (double ice horns and single ice horn). When the droplets collide on the surface of the component, they do not immediately freeze and the water film (formed by droplets) gradually freezes while flowing along the material surface, forming glaze ice. Water film squeezes small air bubbles during the flow, so the ice is transparent and dense. Moreover, due to the aero-heating in the leading-edge area, especially the stagnation point, the thickness of the ice is small, and the large-scale icing occurs behind the two sides of the stagnation point, and it generally forms an ice horn. When near the 0° angle of attack, the ice forms a significant double ice angle; when the angle of attack is near the non-0° angle of attack, there is generally only one obvious angle of ice (main ice angle). In Table 1, the App. C-CM represents the continuous maximum icing conditions in Appendix C of Part 25 of CFR 14. App. O represents CFR 14 Part 25 Appendix

O icing condition, while FZDZ/L is the freezing drizzle (MVD < 40 μm), and FZDZ/G is the continuous maximum icing condition of the freezing drizzle (MVD ≥ 40 μm). FZRA is the icing condition of Appendix O freezing rain. As the 14,000 ft altitude exceeds the envelope of App. O when the static temperature T_s equals to −6.6 °C, altitude was set as H = 5000 ft in the uniform. The value of the median volume diameter (MVD) is taken when the cumulative mass of the droplets reaches 50%. The liquid water content (LWC) takes the maximum value corresponding to Appendix O.

Table 1. Test conditions.

Run No.	H (ft)	V (m/s)	AOA (°)	T_s (°C)	MVD (μm)	LWC (g/m^3)	Time (min)	Cloud
1	14,000	95	4.9	−6.6	20	0.50	11 min	App.C-CM
2	14,000	95	0.0	−6.6	20	0.50	11 min	App.C-CM
3	14,000	95	4.9	−6.6	20	0.40	11 min	App.O-FZDZ/L
4	14,000	95	0.0	−6.6	20	0.40	11 min	App.O-FZDZ/L
5	14,000	95	4.9	−6.6	110	0.25	11 min	App.O-FZDZ/G
6	14,000	95	0.0	−6.6	110	0.25	11 min	App.O-FZDZ/G
7	5900	95	4.9	−6.6	19	0.28	11 min	App.O-FZRA/L
8	5900	95	0.0	−6.6	19	0.28	11 min	App.O-FZRA/L
9	5900	95	4.9	−6.6	526	0.24	11 min	App.O-FZRA/G
10	5900	95	0.0	−6.6	526	0.24	11 min	App.O-FZRA/G

The test conditions in Table 1 are very typical glaze ice icing conditions. In particular, the angle of attack of 4.9 degrees and H = 14,000 ft are the typical angle of attack and altitude in the holding stage of a large aircraft, which will form an obvious upper ice horn (usually on the wing). The angle of attack of 0 degrees will form obvious double ice horns (usually on the horizontal tail). The MVD = 20 μm is the most critical MVD condition after sensitivity analysis in Appendix C in FAR25. Ts = −6.6 °C is very close to the most critical static temperature (−4.1 °C). Considering the problem of ice shedding, Ts is designed to be 2.5 °C lower. The LWC is determined jointly by Ts and MVD in Appendix C in FAR25. As the model is relatively small, the ice accretion is relatively fast, so the icing time cannot reach the holding icing time (in Appendix C in FAR25 holding icing time is 45 min). Considering that the ice horn is easy to break when it is too high, after calculation carried out before the experiment, it was considered that 11 min is appropriate. The MVD value in Appendix O is the MVD when cumulative mass of droplet reaches 0.5, shown in Figures 6 and 7.

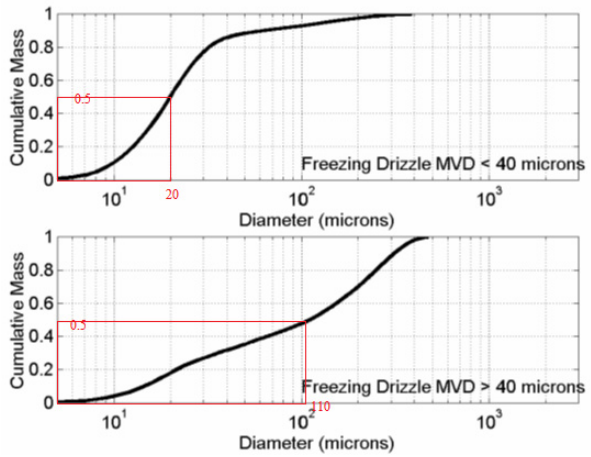

Figure 6. Appendix O—freezing drizzle, drop diameter distribution.

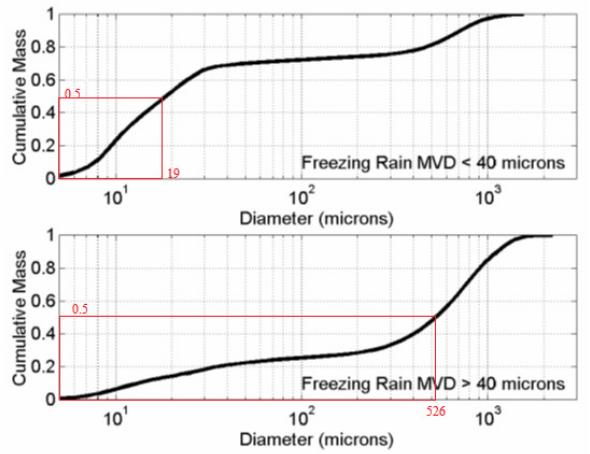

Figure 7. Appendix O—freezing rain, drop diameter distribution.

5. Test Results

The pressure distribution of the leading region in both flight states was matched in the wind tunnel prior to the icing test. The results of the pressure distribution matching results for the two states, AOA = 0° and AOA = 4.9°, are shown in Figures 8 and 9. In Figures 8 and 9, the abscissa x/c (dimensionless) represents relative position in the chordal direction (the c is the length of the airfoil chord). The ordinates Cp represent the dimensionless pressure coefficient.

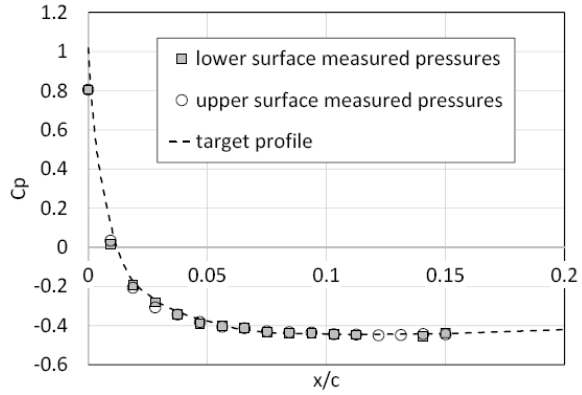

Figure 8. Pressure distribution of the leading−edge matching at AOA = 0°.

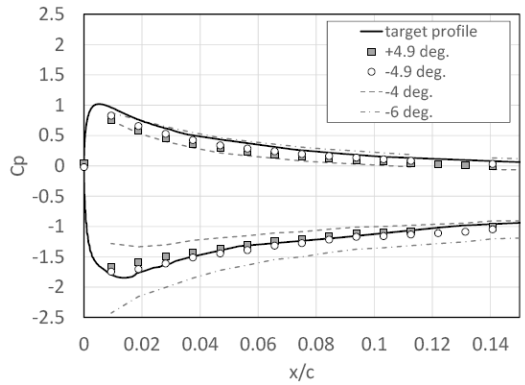

Figure 9. Pressure distribution of the leading−edge matching at AOA = 4.9°.

After pressure distribution matching, icing runs were conducted: first, the wind speed was adjusted to the target wind speed. Second, the air was cooled down to the target

temperature. Third, the nozzle was turned on to spray supercooled droplets and this was timed. Fourth, when the icing time was up, the spray ended. Fifth, the temperature was reduced (to prevent ice from falling off). Sixth, after cooling, the wind was decreased to make the wind speed zero. Seventh, the hatch door was opened, and the "hot knife" (square copper plate, with which the shape of the leading edge of the airfoil was removed) was heated to melt the ice shape, forming a groove (as shown in Figure 10), so that the hot knife could fit with the airfoil. Eighth, the coordinate paper was stuck on the hot knife, and then the ice shape was drawn on the coordinate paper along the circumference of the ice shape. Ninth, the ice was heated to melt it quickly. Tenth, the airfoil surface was cleaned and the next test run was conducted.

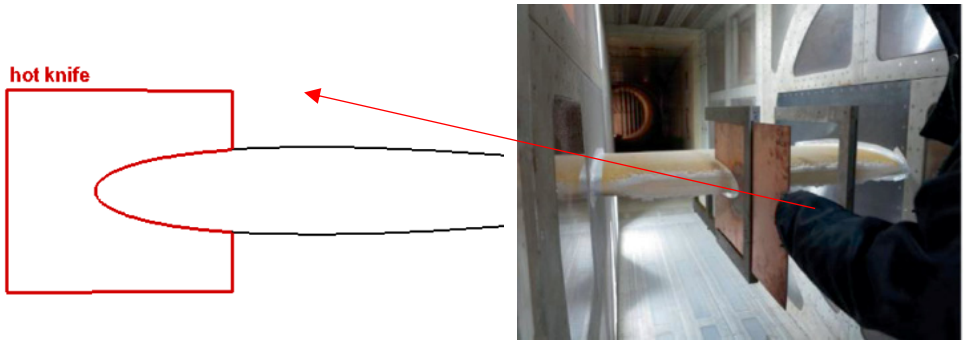

Figure 10. Hot knife used in many icing wind tunnels.

After ice accumulation, ice shapes were taken at three different span locations (center line and 100 mm on the left and right sides of the center of the model as shown in Figure 11 in red curves). The ice shapes at the three different sections coincide in position and height of the ice horn well. The ice shapes presented in this paper were all obtained at the centerline position of the model.

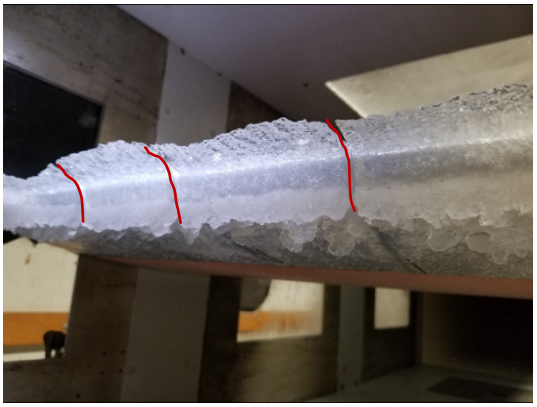

Figure 11. Ice shape at three different span locations.

In Figure 12, ice shapes with a single ice horn in different states are shown in different colors. The main ice horn of Appendix C is the highest, followed by FZDZ/L, FZDZ/G and FZRA/L and FZRA/G. Ice shape of Appendix C has the smallest range of the rough element, and the height of the rough element decreases sharply far away from the main ice horn; the range of the SLD ice shapes after the main ice horn are very large, and the rough element is almost the same in different states; the height of the rough element does not decrease significantly with the distance away from the main ice horn.

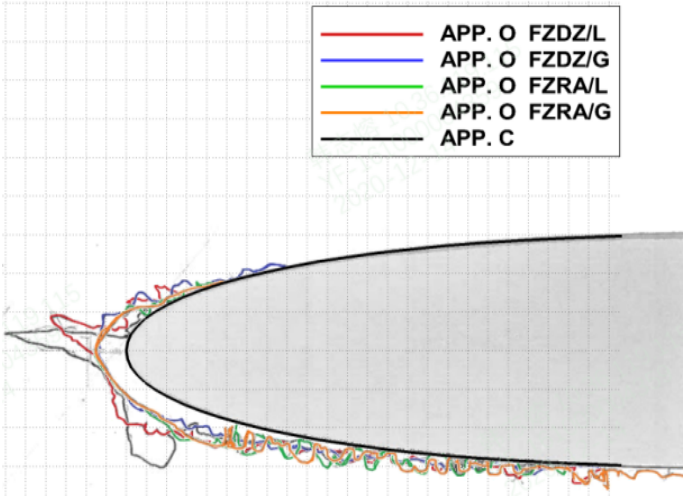

Figure 12. Ice shapes with single horn at AOA = 4.9°.

In Figure 13, ice shapes with double ice horns in different states are shown in different colors. The height of the main ice horns decreases gradually from Appendix C to FZDZ/L, FZDZ/G; while the main ice horn of FZRA/L and FZRA/G is not very obvious. Appendix C has minimized the range of the rough element, and the rough element height decreases sharply far away from the main ice horn; the range of the SLD ice shape after the main ice horn is very large, and the rough element is almost the same in different states; the height of the rough element does not decrease significantly with the distance away from the main ice horn.

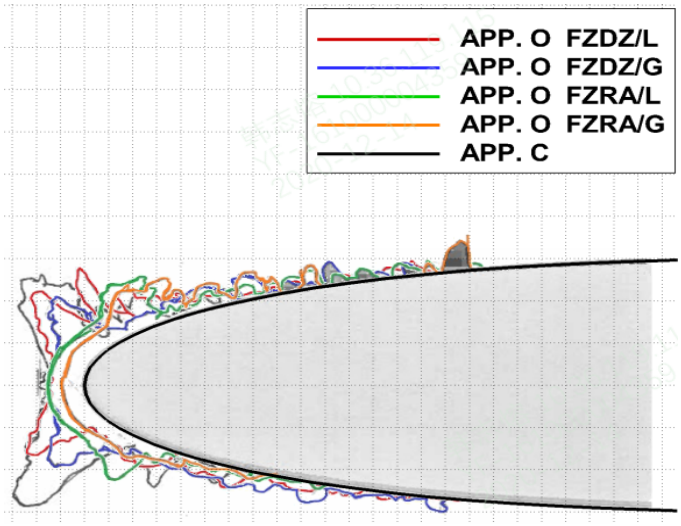

Figure 13. Ice shapes with double horns at AOA = 0°.

Through the comparative analysis of the above test results, it can be seen that a significant result of the SLD icing was ice accretions that formed downstream of the ice-protected surfaces [27]. The shape characteristics of ice in Appendix O are consistent with those in other references [13,19,28,29]. After observing the shape of the roughness element behind the main ice horn shown in Figure 14, the roughness cannot be formed by runback water, it can only be formed by reattachment of water droplet splashing or bouncing [30–33] as shown in Figure 15 because the roughness element particles are discontinuous, as shown in Figure 13.

Figure 14. Ice shape of normal drop (**left**) and SLD (**right**).

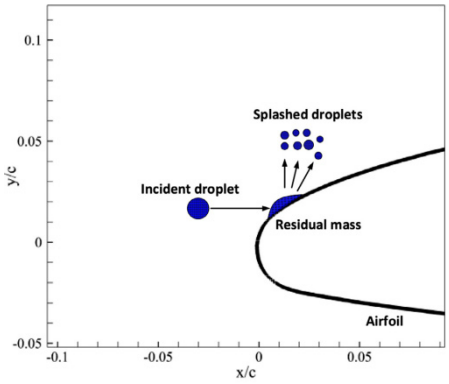

Figure 15. Simplification of droplet splashing for 2D simulation.

The shape characteristics of ice in Appendix O are consistent with those in other references. For example, the test results in NASA IRT and Chinese FL-61 icing wind tunnel. It can be found in the above icing wind tunnel from References [16,19,29,34] that after the main ice horn, the range of roughness element is wide, and there is little ice at the gap between the roughness elements, indicating that the formation of the roughness element here is not due to the runback water, but SLD splashing and bouncing.

6. Conclusions

In NRC's AIWT, the icing wind tunnel test of normal droplets and SLD was carried out. The differences from the comparison of ice shapes were consistent with the splashing and bouncing [30,31] theory of SLD:

(1) As the LWC of SLD is smaller than the LWC of normal droplets, the ice horn height of SLD is smaller than that of the normal droplets. At the same time, due to the splashing and rebound phenomenon of large droplets, the main ice horn of SLD ice will be further reduced, and the position of the main ice horn will move to the trailing edge, especially in the case of freezing rain.

(2) After splashing and rebounding, droplets will continue to fly to the trailing edge with the airflow. Due to the influence of gravity and airflow, some droplets will hit the airfoil twice, thus forming rough elements in a far range after the main ice horn of the leading edge. This rough element is mainly caused by the splashing and rebound of droplets, rather than the runback water, so the height of the rough element does not decrease significantly with the distance away from the main ice angle, and obvious discontinuities between rough elements will occur.

Author Contributions: Conceptualization and methodology, Z.H.; methodology, J.S.; resources and data curation, D.W.; writing—original draft preparation, Z.H.; writing—review and editing, J.S.; supervision, D.W.; project administration, Z.H.; funding acquisition, J.S. All authors have read and agreed to the published version of the manuscript.

Funding: This research was funded by the National Key R&D Program of China (Project No. 2020YFA0712000).

Conflicts of Interest: The authors declare that they have no known competing financial interest or personal relationships that could have appeared to influence the work reported in this paper.

References

1. Appiah-Kubbi, P.; Martos, B.; Atuahene, I.; William, S. U. S. inflight icing accidents and incidents, 2006 to 2010. In Proceedings of the Industrial and Systems Engineering Research Conference, San Juan, Puerto Rico, USA, 18–22 May 2013.
2. Johnson, C.L. Wing loading, icing and associated aspects of modern transport design. *J. Aeronaut. Sci.* **1940**, *8*, 43–54. [CrossRef]
3. Gulick, B.G. *Effects of Simulated Ice Formation on the Aerodynamic Characteristics of an Airfoil*; Technique Report L292; NACA: Washington, DC, USA, 1938.
4. Ashenden, R.; Lindberg, W.; Marwitz, J.D.; Hoxie, B. Airfoil performance degradation by supercooled cloud drizzle and rain drop icing. *AIAA J. Aircr.* **1996**, *33*, 1040–1046. [CrossRef]
5. Lee, S.; Bragg, M.B. Experimental investigation of simulated large-droplet ice shapes on airfoil aerodynamics. *AIAA J. Aircr.* **1999**, *36*, 844–850. [CrossRef]
6. Bragg, M.B.; Broeren, L.A.; Blumenthal, A.P. Iced-airfoil aerodynamics. *Prog. Aerosp. Sci.* **2005**, *41*, 323–362. [CrossRef]
7. Federal Aviation Administration. *Part 25: Airworthiness Standard: Transport Category Airplanes, Admt 25-140. Title 14: Aeronautics and Space. U.S.*; Federal Aviation Administration: Washington, DC, USA, 2014.
8. European Union Aviation Safety Agency. *CS-25: Certification Specifications and Acceptable Means of Compliance for Large Aeroplanes, Admt 27*; European Union Aviation Safety Agency: Cologne, Germany, 2021.
9. Bragg, M.B.; Perkins, W.; Sarter, N.; Basar, T.; Voulgaris, P.; Gurbacki, H.; Melody, J.; McCray, S. An interdisciplinary approach to inflight aircraft icing safety. In Proceedings of the 36th AIAA Aerospace Sciences Meeting and Exhibit, Reno, NV, USA, 12–15 January 1998.
10. Fu, C.; Song, W.; Peng, Q.; Liao, D.; Wang, C. An overview of supercooled large droplets icing condition simulation capacity in icing wind tunnels. *J. Exp. Fluid Mech.* **2017**, *31*, 1–7.
11. Judith, F.; Van, Z.; IDE, R.F. NASA Glenn Icing Research Tunnel: 2012 cloud calibration procedure and results. In Proceedings of the 4th AIAA Atmospheric and Space Environments Conference, New Orleans, LA, USA, 25–28 June 2012.
12. Steen, L.E.; IDE, R.F. NASA Glenn Icing Research Tunnel: 2014 and 2015 Cloud Calibration Procedures and Results. NASA/TM—2015-218758. 2015. Available online: https://ntrs.nasa.gov/citations/20150009300 (accessed on 24 November 2022).
13. Potapczuk, M.G.; Tsao, J.C.; King-Steen, L.E. Bimodal SLD ice accretion on a NACA 0012 airfoil model. In Proceedings of the 9th AIAA Atmospheric and Space Environments Conference, Denver, CO, USA, 5–9 June 2017.
14. Potapczuk, M.G.; Tsao, J. Bimodal SLD ice accretion on swept NACA0012 airfoil models. In Proceedings of the AIAA AVIATION 2020 FORUM, Virtual Event, 15–19 June 2020.
15. Esposito, B.M.; Ragni, A.; Ferrigno, F.; Vecchione, L. Cloud Calibration Update of the CIRA Icing Wind Tunnel. SAE Technical Paper Series. In Proceedings of the FAA In-Flight Icing/Ground De-icing International Conference & Exhibition, Chicago, IL, USA, 16–20 June 2003. [CrossRef]
16. Shu, J.; Xu, D.; Han, Z.; Li, S.; Huang, X. Study on the hybrid wing design of the icing wind tunnel SLD icing test. *Acta Aeronaut. Astronaut. Sin.* **2023**, *44*, 627182. (In Chinese) [CrossRef]
17. Fu, C.; Peng, Q.; Zhang, H.; Wang, C.; Wu, S. Preliminary research on spray nozzle atomization characteristics in icing wind tunnel environment. *J. Exp. Fluid Mech.* **2015**, *29*, 30–34.
18. Potapczuk, M. SLD Research at NASA: Basic Research. NASA Rep. 2015-0007676. Presented to WEZARD SLD Workshop Brussels, Belgium, 10 June 2013. Available online: https://ntrs.nasa.gov/api/citations/20150007676/downloads/20150007676.pdf (accessed on 24 November 2022).
19. William, B.W.; Mark, G.P.; Laurie, H.L. Comparison of LEWICE and GlennICE in the SLD regime. In Proceedings of the 46th AIAA Aerospace Sciences Meeting and Exhibit, Reno, Nevada, 7–10 January 2008.
20. Bidwell, C. Icing Simulation. NASA/CP-2009-215797, NASA Glenn Research Center. 2009; pp. 71–86. Available online: https://ntrs.nasa.gov/api/citations/20090030605/downloads/20090030605.pdf (accessed on 24 November 2022).
21. Oleskiw, M.M.; Hyde, F.H.; Penna, P.J. In-flight icing simulation capabilities of NRC's altitude icing wind tunnel. In Proceedings of the 39th Aerospace Sciences Meeting and Exhibit, Reno, NV, USA, 8–11 January 2001.
22. Orchard, D.; Clark, C.; Oleskiw, M. Development of a supercooled large droplet environment within the NRC Altitude Icing Wind Tunnel. In Proceedings of the SAE 2015 International Conference on Icing of Aircraft, Engines, and Structures, Prague, Czech Republic, 22–25 June 2015; SAE Technical Paper: Warrendale, PA, USA, 2015. [CrossRef]
23. Orchard, D.; Clark, C.; Chevrett, G. Measurement of liquid water content for supercooled large drop conditions in the NRC's altitude icing wind tunnel. In Proceedings of the International Conference on Icing of Aircraft, Engines, and Structures, Minneapolis, MN, USA, 17–21 June 2019; SAE Technical Paper: Warrendale, PA, USA, 2019. [CrossRef]
24. Orchard, D.; Szlider, K.; Davison, C. Design of an icing wind tunnel contraction supercooled large drop conditions. In Proceedings of the 2018 Atmospheric and Space Environments Conference, Atlanta, Georgia, 25–29 June 2018.
25. Heinrich, A.; Ross, R.; Zumwalt, G.; Provorse, J.; Padmanabhan, V. *Aircraft Icing Handbook*; ADA238040, DOT/FAA/CT-88/8-2; Federal Aviation Administration: Washington, DC, USA, 1991.
26. Cornell, D.; Donahue, C.A.; Keith, C. A Comparison of Aircraft Icing Forecast Models. Technical Note, AFCCC/TN-95/004. 1995. Available online: https://apps.dtic.mil/sti/pdfs/ADA303307.pdf (accessed on 24 November 2022).

27. Miller, D.R.; Addy, H.E., Jr.; Ide, R.F. A study of large droplet ice accretions in the NASA-Lewis IRT at near-freezing conditions. In Proceedings of the 34th Aerospace Sciences Meeting and Exhibit, Reno, NV, USA, 15–18 January 1996.
28. Tsao, J.C. Additional results of glaze icing scaling in SLD conditions. In Proceedings of the 8th AIAA Atmospheric and Space Environments Conference, Washington, DC, USA, 13–17 June 2016.
29. Potapczuk, M.G.; Tsao, J.C. Further examinations of bimodal SLD ice accretion in the NASA icing research tunnel. In Proceedings of the 2018 Atmospheric and Space Environments Conference, Atlanta, Georgia, 25–29 June 2018.
30. Wright, W.B.; Potapczuk, M.G. Semi-empirical modeling of SLD physics. In Proceedings of the 42nd AIAA Aerospace Sciences Meeting and Exhibit, Reno, Nevada, 5–8 January 2004.
31. Tan, S.C. A tentative mass loss model for simulating water droplet splash. In Proceedings of the 42nd AIAA Aerospace Sciences Meeting and Exhibit, Reno, Nevada, 5–8 January 2004.
32. Trujillo, M.F.; Mathews, W.S.; Lee, C.F.; Peters, J.E. Modeling and experiment of impingement and atomization of a liquid spray on a wall. *Int. J. Engine Res.* **2000**, *1*, 87–104. [CrossRef]
33. Bilodeau, D.R.; Habashi, W.G.; Fossati, M.; Baruzzi, G.S. Eulerian modeling of supercooled large droplet splashing and bouncing. *J. Aircr.* **2015**, *52*, 1611–1624. [CrossRef]
34. Potapczuk, M.G.; Tsao, J.C. The Influence of SLD Drop Size Distributions on Ice Accretion in the NASA Icing Research Tunnel. In Proceedings of the International Conference on Icing of Aircraft, Engines, and Structures, Minneapolis, MN, USA, 17 June 2019.